Rydberg-valence mixing and interchannel coupling in resonant oxygen 1*s* inelastic x-ray scattering of O_2

Victor Kimberg,[1,2] Tatsuo Gejo,[3,4] Masaki Oura,[3] Takashi Tokushima,[3] Yuka Horikawa,[3] Hidemi Arai,[3] Shik Shin,[3,5] and Nobuhiro Kosugi[2,*]

[1]*Max Planck Institute for the Physics of Complex Systems, Dresden, c/o DESY, Hamburg 22607, Germany*
[2]*Institute for Molecular Science, Myodaiji, Okazaki, Aichi 444-8585, Japan*
[3]*RIKEN SPring-8 Center, Kouto, Sayo-gun, Hyogo 679-5148, Japan*
[4]*Department of Material Science, University of Hyogo, Kouto, Ako-gun, Hyogo 678-1297, Japan*
[5]*Institute for Solid State Physics, University of Tokyo, Kashiwano-ha, Kashiwa, Chiba 277-8581, Japan*

(Received 27 January 2011; published 5 March 2012)

Rydberg-valence (RV) mixing and doublet-quartet (DQ) interchannel coupling in the core-excited states of triplet open-shell O_2 are experimentally and theoretically unveiled through the resonant inelastic x-ray scattering around the O 1$s \rightarrow \sigma_u^*$ resonance. *Ab initio* calculations explain complicated excitation energy dependence of the spectral profile by the interplay of the DQ interchannel coupling under the presence of the RV mixing. Complicated intermediate states with valence and/or Rydberg character are successfully analyzed through the filtering of pure valence and pure Rydberg final states.

DOI: 10.1103/PhysRevA.85.032503 PACS number(s): 33.20.Rm, 31.15.A−, 31.50.Gh, 33.70.Fd

I. INTRODUCTION

Nonadiabatic interaction between potential energy surfaces of different electronic states is a fundamental phenomenon to determine dynamical processes including the coupling of nuclear motion with electronic states (vibronic or electron–molecular-vibration coupling) in physics, chemistry, and biology. However, interaction even between two states has not yet been fully understood [1]. Recently, by using femtosecond lasers, control of chemical reactions in a simplified system is made possible and even artificial potential energy curve (PEC) crossings can be manipulated under intense laser fields [2]. To carry out such advanced studies of complicated excitation dynamics, we need to accumulate detailed information on the interaction of PECs experimentally and theoretically. We can now use not only lasers but also intense x rays from recently available high-brilliant synchrotron radiation and free electron lasers. The PEC crossing between bound and dissociative states is one of the most fundamental interactions. The core-to-Rydberg and σ^* valence excited states are typically bound and dissociative [3]. O_2 has a weak σ bond in the triplet ground state ($^3\Sigma_g^-$) and its O 1$s \rightarrow \sigma_u^*$ ($3\sigma_u^*$) excitation level is lowered into the Rydberg region. Then, x-ray absorption spectroscopy (XAS) shows extremely complicated spectral features due to the Rydberg-valence (RV) curve crossings in the doublet ($^2\Sigma_{g,u}^-$) and quartet ($^4\Sigma_{g,u}^-$) ionization manifolds [4,5]. In the present work, we use intense tunable soft x-rays to observe resonant inelastic x-ray scattering (RIXS) from the core-excited states and successfully analyzed not only the RV interaction but also the doublet-quartet (DQ) interchannel coupling in the doublet and quartet ionization manifolds [6]. Our idea is to observe RIXS between these complicated intermediate states and several well-characterized final states after the symmetry-selective dipole transition. Based on a similar idea, resonant photoemission between the intermediate and final states has been measured but its analysis is not straightforward or conclusive between the neutral excited state and the ionized state after the nondipole Auger decay [7–9]. Very recently, a high-resolution RIXS profile of O_2 demonstrates spatial quantum beats caused by interference between scattering channels through the two (doublet and quartet) core-hole dissociative states [10]. However, the contribution from Rydberg states is not discussed from the viewpoint of the RV mixing. The importance of both the RV mixing and DQ interchannel coupling has not yet been recognized in O 1*s* RIXS of O_2 [10–13], though recent progress of synchrotron radiation sources and soft x-ray emission spectrometers makes RIXS an excellent tool to reveal the excitation dynamics of the intermediate and final states in the second-order optical process.

II. EXPERIMENT

Figure 1 displays the present O 1*s* RIXS spectra of O_2, showing strong incident photon energy ($h\nu_{in}$) dependence. The RIXS spectra were measured by using a high-performance slitless spectrometer equipped with the compact flange-mounted liquid and gas flow cell with a 150-nm-thick Au-coated SiC membrane window [14]. The spectrometer is installed at the a branch of the soft x-ray undulator beamline BL17SU, SPring-8 [15,16]. The energy resolution of the incident photon beam was set to be about 65 meV at 530 eV, and its degree of circular polarization P_c was about 0.98. The use of circular polarization light ensures that the RIXS cross sections are free from the anisotropy effects. The energy calibration was done by measuring total ion-yield XAS spectra of O_2 gases.

III. THEORY

The intermediate states in the RIXS process of O_2 ($X\ ^3\Sigma_g^-$) have the $^3\Sigma_u^-$ and $^3\Pi_u$ symmetries and have O 1*s* ion core channels of four different symmetries $^4\Sigma_{g,u}^-$ and $^2\Sigma_{g,u}^-$ (hereafter denoted simply by [$Q_{g,u}$] and [$D_{g,u}$]). Then, the final states have the $^3\Sigma_g^-$ and $^3\Pi_g$ symmetries and have valence ion core channels of eight different symmetries: quartet and doublet, Π and Σ^-, and gerade and ungerade. The XAS

*kosugi@ims.ac.jp

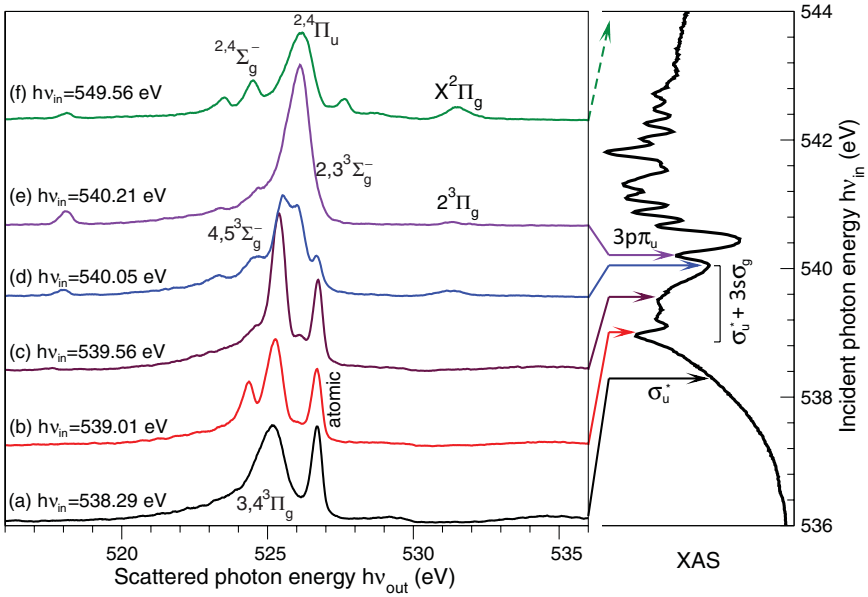

FIG. 1. (Color online) Experimental RIXS (left) and XAS (right) spectra. The incident photon energies $h\nu_{\rm in}$ are shown with arrows on the XAS near the O $1s \rightarrow \sigma_u^*$ resonance. $h\nu_{\rm in} = 538.29$ eV (a), 540.21 eV (e), and 549.56 eV (f) correspond to the excitation to the pure $\sigma_u^*[{\rm D}_g]$ valence, the pure $3p\pi_u[{\rm Q}_g]$ Rydberg state, and the ${}^4\Sigma_{g,u}^-({\rm Q}_{g,u})$ and ${}^2\Sigma_{g,u}^-({\rm D}_{g,u})$ ionization continuum, respectively [4,23]. $h\nu_{\rm in} = 539.01$ eV (b), 539.56 eV (c), and 540.05 eV (d) correspond to the excitation to different RV mixed states of $\sigma_u^*[{\rm D}_g]$, $\sigma_u^*[{\rm Q}_g]$, $3s\sigma_g[{\rm Q}_u]$, and $3s\sigma_g[{\rm D}_u]$ [6]. Some XAS and RIXS assignments are shown; for the detailed assignment, refer to the text and Fig. 4.

spectrum shown in Fig. 1 includes the O $1s$ resonant excitation to the valence-type state $\sigma_u^*[{\rm D}_g]$ and the $3s\sigma_g$, $3p\sigma_u$, and $3p\pi_u$ Rydberg-type states, and also the off-resonant excitation above the O $1s$ ionization thresholds 543.4 eV ($Q_{g,u}$) and 544.4 eV ($D_{g,u}$). Following the previous discussion [17], $\sigma_u^*[{\rm D}_g]$ is based on the picture of the diabatic representation for the σ_u^* electron bound in the D_g (${}^2\Sigma_g^-$) channel but can be coupled with $\sigma_u^*[{\rm Q}_g]$ within the same dipole-allowed ${}^3\Sigma_u^-$ symmetry. In the Rydberg states, the DQ interchannel coupling among $[{\rm Q}_g]$, $[{\rm Q}_u]$, $[{\rm D}_g]$, and $[{\rm D}_u]$ is quite small, though the $3p\sigma_u[{\rm Q}_g]$ Rydberg state is strongly mixed with the $\sigma_u^*[{\rm Q}_g]$ state having the DQ interchannel coupling with the $\sigma_u^*[{\rm D}_g]$ in the Franck-Condon region [6].

Figure 2 shows *ab initio* PECs of the core and valence ionized states, responsible for the off-resonant x-ray emission spectrum [Fig. 1(f)]. Figure 3 shows *ab initio* PECs of the core and valence excited states, responsible for the RIXS spectra shown in Figs. 1(a)–1(e). The splitting between core-ionized gerade and ungerade states in *ab initio* predictions using the symmetry-adapted molecular orbitals (MOs) is very small in O_2 (0.03 eV in ${}^4\Sigma^-$ and 0.004 eV in ${}^2\Sigma^-$ [18]), which rationalizes the use of the same PECs obtained using the localized core orbital for gerade and ungerade channels. Therefore, the core ionized and core excited state PECs [Figs. 2(a) and 3(a)] were taken from the previous configuration interaction (CI) calculations using the localized core orbitals [4,6], which show faster convergence to variationally lower energies. On the other hand, the valence ionized and excited-state PECs [Figs. 2(b) and 3(b)] corresponding to the final states of the off-resonant x-ray emission and RIXS processes were calculated using the ground-state (delocalized) MOs. The basis set and CI scheme was the same as the previous one [6] using the GSCF3 program package [19,20]. Since the CI calculations using the ground-state MOs show very slow convergence to describe the core ionized and excited states, the transition dipole moment was regarded as independent of the internuclear distance. In addition, some small energy shifts (0.5–1.0 eV) in the final state PECs were introduced.

IV. COMPARISON BETWEEN EXPERIMENT AND THEORY

Figure 4 shows the theoretical RIXS and off-resonant spectra obtained by the time-dependent solution of the Schrödinger equation [21,22] using the PECs shown in Figs. 2 and 3. This approach treats the resonant x-ray scattering as the one-step process and allows us to take into explicit account the vibronic (or nonadiabatic) coupling in the intermediate core-excited state [6] and the DQ interchannel coupling. Let us first discuss the off-resonant x-ray emission spectrum at $h\nu_{\rm in} = 549.56$ eV in Fig. 1(f). There are four possible intermediate core-ionized states ${}^4\Sigma_g^-$, ${}^4\Sigma_u^-$, ${}^2\Sigma_g^-$, and ${}^2\Sigma_u^-$. In the case of the off-resonant condition, all the scattering channels are independent and the total spectrum is obtained as a superposition of the individual channels. Theoretical off-resonant x-ray emission spectra are shown in Fig. 4(f), where the lifetime broadening of the core-ionized state at HWHM is 80 meV (Lorentzian) and the instrumental broadening at HWHM is 250 meV (Gaussian). Each peak assignment is the same as the previous one [11]. The low-lying valence ionized states with the binding energy (ionization energy) of 12–25 eV are $X\,{}^2\Pi_g$, $a\,{}^4\Pi_u$, $A\,{}^2\Pi_u$, $b\,{}^4\Sigma_g^-$, $B\,{}^2\Sigma_g^-$, and $c\,{}^4\Sigma_u^-$, where the scattered photon energies $h\nu_{\rm out}$ for the quartet and doublet final states are determined relative to the quartet and doublet ionization thresholds, 543.4 eV ($Q_{g,u}$) and 544.4 eV ($D_{g,u}$), respectively. The theoretical intensity of the $X\,{}^2\Pi_g$ final state is overestimated due to the accidental self-absorption effect in the vicinity of the O $1s \rightarrow \pi_g^*(1\pi_g)$ resonance energy ($h\nu_{\rm in} = 530-531.5$ eV) in the experimental spectrum. A small peak around $h\nu_{\rm in} = 527.5$ eV (as well as another smaller and broader peak at $h\nu_{\rm out} = 528.7$ eV) is not found in the *ab initio* calculations. It is shown experimentally that this feature increases the intensity with the increase of the excitation photon energy (not shown here) and is dependent on the excitation source, photons or electrons [11]. Therefore, the satellite features of $h\nu_{\rm out} = 527-529$ eV in the off-resonant spectra may arise from the x-ray scattering processes involving shake-up states.

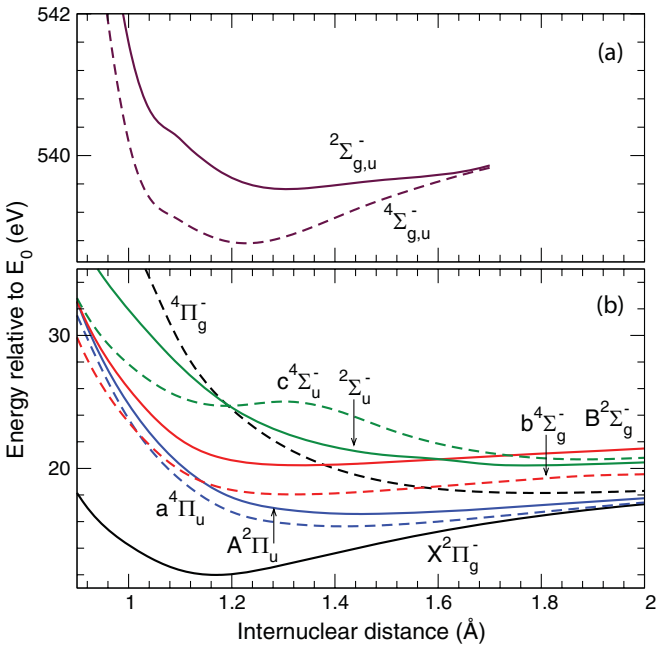

FIG. 2. (Color online) PECs for the electronic states responsible for the off-resonant x-ray scattering. Panels (a) and (b) show intermediate core-ionized states and final singly ionized valence states, respectively, where solid lines denote doublet states and dashed lines denote quartet states. The energy is relative to the minimum energy E_0 of the ground-state PEC.

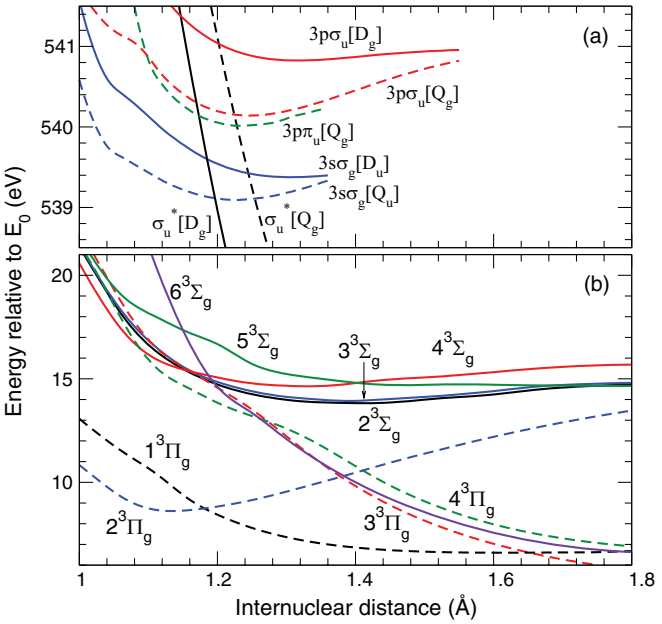

FIG. 3. (Color online) PECs for the electronic states responsible for the resonant x-ray scattering. Panels (a) and (b) show intermediate core-excited states and final valence-excited states, respectively. The energy is relative to the minimum energy E_0 of the ground-state PEC.

V. DISCUSSION

Let us now discuss the RIXS feature and its $h\nu_{\rm in}$ dependence. The RIXS profiles are well reproduced with the help of the wave-packet simulation as shown in Fig. 4. However, the long tail to the lower emission energy observed in all the experimental spectra is not reproduced and may arise from several highly (multiply) excited states with small transition probabilities, which are not included in the present PEC calculations. For the excitation energies $h\nu_{\rm in}$ = 538–540 eV [Figs. 1(a)–1(d)] at the $1s \rightarrow \sigma^*_u$ resonance, the intermediate states are complicated; that is, in the dipole transition to $^3\Sigma^-_u$ and $^3\Pi_u$ states from the $X\,^3\Sigma^-_g$ ground state of O_2, we have to take into account the valence states, $\sigma^*_u[{\rm D}_g]$ and $\sigma^*_u[{\rm Q}_g]$, and the Rydberg states, $3s\sigma_g[{\rm Q}_u]$, $3s\sigma_g[{\rm D}_u]$, and $3p\sigma_u[{\rm Q}_g]$ in the $^3\Sigma^-_u$ manifold, and an isolated Rydberg state $3p\pi_u[{\rm Q}_g]$ in the $^3\Pi_u$manifold [23]. As shown in Fig. 3(a), the core-excited valence σ^*_u states interact nonadiabatically with the $3s\sigma_g$ and $3p\sigma_u$ Rydberg states near the Franck-Condon region (R∼1.2 Å) [6]. In order to understand the detailed RV mixing effects in the RIXS profile, we have chosen five typical excitation energies around the $1s \rightarrow \sigma^*_u$ resonance as captioned in Fig. 1. Figure 3(b) shows PECs of some low-lying valence-excited $^3\Sigma^-_g$ and $^3\Pi_g$ states. The lowest $1^3\Pi_g$ and 2 $^3\Pi_g$ excited states with the $3\sigma_g \rightarrow 1\pi^*_g$ and $1\pi^*_g \rightarrow 3s\sigma_g(3s\sigma_g[X\,^2\Pi_g])$ configurations were discussed by Lewis *et al.* [24], but other $^3\Sigma^-_g$ and $^3\Pi_g$ states responsible for the RIXS features have not yet been discussed. In the $^3\Sigma^-_g$ manifold, the excited states with the $3p\pi_u[a\,^4\Pi_u, A\,^2\Pi_u]$, $3s\sigma_g[b\,^4\Sigma^-_g, B\,^2\Sigma^-_g]$, $3p\sigma_u[c\,^4\Sigma^-_u]$, and $\sigma^*_u[c\,^4\Sigma^-_u]$ configurations are contributive to the RIXS feature; on the other hand, in the $^3\Pi_g$ manifold, the excited states with the $3s\sigma_g[X\,^2\Pi_g]$, $3p\sigma_u[a\,^4\Pi_u, A\,^2\Pi_u]$, $\sigma^*_u[a\,^4\Pi_u, A\,^2\Pi_u]$, and $3p\pi_u[c\,^4\Sigma^-_u]$ configurations are contributive.

Figures 1(a)–1(c) shows a rather sharp peak at $h\nu_{\rm out}$ = 526.7 eV. The present CI calculations do not show such a low-lying molecular state. The energy position of this peak is not dependent on the excitation photon energies $h\nu_{\rm in}$, and it disappears when $h\nu_{\rm in}$ is tuned to the bound $3p\pi_u$ Rydberg state with no contribution from σ^*_u $[3p\pi_u[{\rm Q}_g]$; Fig. 1(e)]. It allows us to assign this peak to an atomic emission O^* $(1s2s^22p^5\,^3P) \rightarrow$ O $(1s^22s^22p^4\,^3P)$ after the ultrafast dissociation along the repulsive σ^*_u state. This atomic transition is discussed in a recent high-resolution RIXS measurement [10]; the ultrafast dissociation is also found in the atomic Auger transition of O^* $(1s2s^22p^5\,^3P)$ [25]. The atomic peak is simulated in Fig. 4 by using a Gaussian function.

The main RIXS feature (1) with $h\nu_{\rm out}$ = 525.2 eV is dominant for the resonance energy $h\nu_{\rm in}$ = 538.3 eV, as shown in Fig. 4(a), and is assigned to the transition from the pure valence state $\sigma^*_u[{\rm D}_g]$ with a small contribution of $\sigma^*_u[{\rm Q}_g]$ to the valence final states $3\,^3\Pi_g$ and $4\,^3\Pi_g$ shown in Fig. 3, where $3\,^3\Pi_g$ and $4\,^3\Pi_g$ have main configurations of $\sigma^*_u[A\,^2\Pi_u]$ and $\sigma^*_u[a\,^4\Pi_u]$ and the transition probabilities are mainly given by $[{\rm D}_g] \rightarrow [A\,^2\Pi_u]$ and $[{\rm Q}_g] \rightarrow [a\,^4\Pi_u]$. The scattered photon energies $h\nu_{\rm out}$ of the final states $3\,^3\Pi_g$ and $4\,^3\Pi_g$ are smaller than the off-resonant x-ray emission to the final states $A\,^2\Pi_u$ and $a\,^4\Pi_u$. This means the binding energy (term value) of the σ^*_u electron in the valence ion cores $A\,^2\Pi_u$ and $a\,^4\Pi_u$ is smaller than that in the O1s ion cores $^4\Sigma^-_g$ and $^2\Sigma^-_g$, as indicated in Fig. 3.

In addition to the main RIXS feature (1), two side features are found at $h\nu_{\rm out}$ = 524.4 eV (2) and 526.1 eV (3). The intensities of the side features are strongly dependent on the excitation energy. Feature (3) is growing up to the

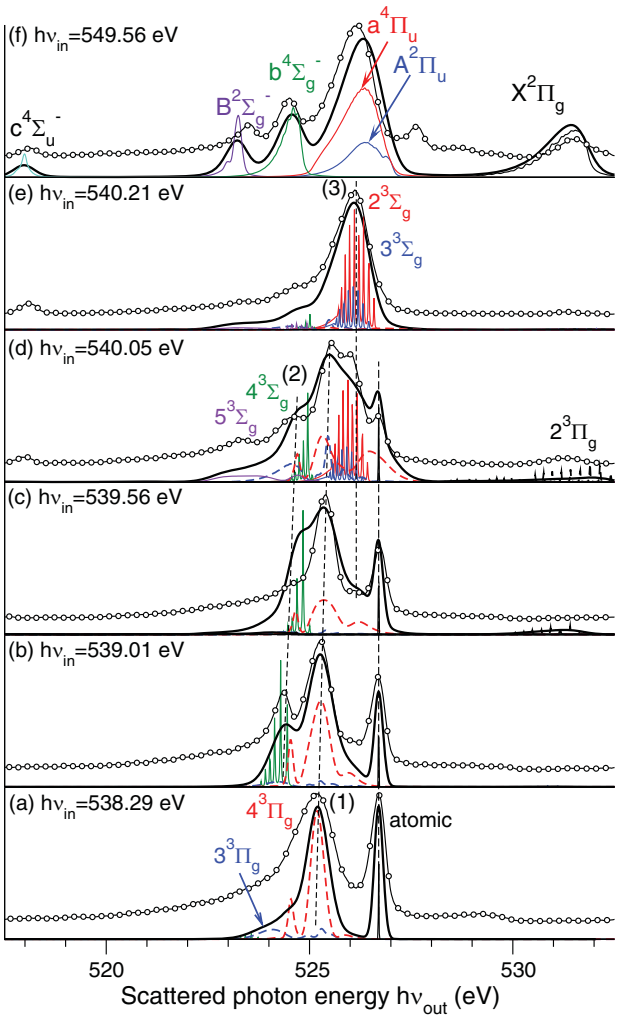

FIG. 4. (Color online) Theoretical simulations of the incident photon energy dependence of the RIXS spectra (a)–(e) near the $1s \rightarrow \sigma_u^*$ resonance in O_2, in comparison with the experimental spectra (circles). The final states observed are strongly dependent on the character of the intermediate states. The off-resonant x-ray emission spectra (f) are also shown. The vibrational structure is smeared out in the off-resonant case due to large lifetime broadening in the core-ionized state.

resonance energy $h\nu_{\rm in} = 540.21$ eV, as shown in Fig. 4(e). The resonance at $h\nu_{\rm in} = 540.21$ eV in the XAS spectrum corresponds to the pure $3p\pi_u[Q_g]$ Rydberg state. Feature (3) is assigned to the transitions to the $2\,^3\Sigma_g^-$ and $3\,^3\Sigma_g^-$ Rydberg states with main configurations of $3p\pi_u[A\,^2\Pi_u]$ and $3p\pi_u[a\,^4\Pi_u]$character. The transition probabilities are mainly given by $[Q_g] \rightarrow [a\,^4\Pi_u]$. The RIXS feature at $h\nu_{\rm out} = 526.1$ eV is almost the same as the off-resonant x-ray emission energy to $A\,^2\Pi_u$ and $a\,^4\Pi_u$ in Fig. 4(f). This is reasonable considering the binding energy (term value) of the Rydberg electron in the valence ion core is almost the same as in the O1s ion core.

On the other hand, the lower energy feature (2) appears when the excitation energy is tuned to the main peak in the XAS resonance band $h\nu_{\rm in} = 539.01$ eV [Fig. 4(b)], corresponding to the intermediate state of dominant $3s\sigma_g[Q_u]$ character. The final state is $4\,^3\Sigma_g^-$ with a main configuration of $3s\sigma_g[b\,^4\Sigma_g^-]$ and the transition probability is mainly given by $[Q_u] \rightarrow [b\,^4\Sigma_g^-]$. The RIXS features with $h\nu_{\rm out} = 523.2$ and 531.5 eV are clearly observed at $h\nu_{\rm in} = 540.05$ eV [Fig. 4(d)]. The final states are $5\,^3\Sigma_g^-$ and $2\,^3\Pi_g$ with main configurations of $3s\sigma_g[B\,^2\Sigma_g^-]$ and $3s\sigma_g[X\,^2\Pi_g]$, respectively, and the transition probability is mainly given by $[D_u] \rightarrow [B\,^2\Sigma_g^-]$ and $[X\,^2\Pi_g]$, indicating the $3s\sigma_g[D_u]$ state shown in Fig. 3 is contributive to this excitation energy in the XAS spectra. The RIXS features at $h\nu_{\rm out} = 524.4$, 523.2, and 531.5 eV are almost the same as the off-resonant x-ray emission energy to $b\,^4\Sigma_g^-$, $B\,^2\Sigma_g^-$, and $X\,^2\Pi_g$ [Fig. 4(f)], respectively. This is reasonable considering the Rydberg character as above mentioned. The intensity of feature (2) decreases rapidly as $h\nu_{\rm in}$ becomes larger than the $1s \rightarrow \sigma_u^*$ resonance (above 540 eV). The appearance of this resonance in the RIXS profile is a direct consequence of the $3s\sigma_g$ Rydberg component in the core-excited states. In this regard, Fig. 4(c) indicates the $3s\sigma_g[Q_u]$ Rydberg component is overestimated at $h\nu_{\rm in} = 539.56$ eV in the CI calculations of the intermediate core-excited states.

There are still some unassigned RIXS features in Figs. 1 and 4. Figures 1(d) and 1(e) show a peak near the off-resonant $c\,^4\Sigma_u^-$ peak position, indicating the contributions of $3p\pi_u[c\,^4\Sigma_u^-]$ and $3p\sigma_u[c\,^4\Sigma_u^-]$ in the final state and of $3p\pi_u[Q_u]$ and $3p\sigma_u[Q_u]$ in the intermediate state. Figure 1(c) shows a very weak feature below the $c\,^4\Sigma_u^-$ peak position, indicating the contributions of $\sigma_u^*[c\,^4\Sigma_u^-]$ in the final state and of $\sigma_u^*[Q_u]$ in the intermediate state by considering different binding energies (term values) in the valence and O 1s ion cores. The weak feature at $h\nu_{\rm out} \approx 530$ eV in Fig. 1(a) may correspond to the inelastic scattering by the $1^3\Pi_g$ excited state of repulsive valence character, as shown in Fig. 3(b), which is more clearly observed on the $1s \rightarrow \pi_g^*$ resonance [13].

VI. CONCLUSIONS

In conclusion, we have studied the RV mixing and DQ interchannel coupling effects at the $1s \rightarrow \sigma_u^*$ resonance in O_2 in the framework of the RIXS. The resonant excitations to the complicated intermediate states as well as the off-resonant excitation have been compared. The dominant final excited states observed in the RIXS are spectatorlike valence excited states, where any strong RV mixings in the final states are not found. It makes it simpler to characterize complicated core-excited states of Rydberg and/or valence character. Complicated RV mixings and DQ interchannel couplings in the intermediate O 1s excited states of O_2 are unveiled through the filtering of pure valence and pure Rydberg final states in the incident photon energy dependence of the RIXS spectra.

ACKNOWLEDGMENTS

One of the authors (V.K.) is grateful for kind support and fruitful discussion by Dr. Catalin Miron during staying at SOLEIL and for JSPS Postdoctoral Fellowship for Foreign Researches (No. 06F06068) during staying in IMS. Part of this work is supported by the JSPS Grant-in-Aids for Scientific

Research (Nos. 19850029 and 20350014). The synchrotron radiation experiments at BL17SU in SPring-8 were performed with the approval of RIKEN (Proposal No. 20070113 and 20080029).

[1] H. Nakamura, *Nonadiabatic Transition. Concepts, Basic Theories and Applications* (World Scientific, Singapore, 2002).
[2] F. C. De Schryver, S. De Feyter, and G. Schweitzer (editors), *Femtochemistry* (Wiley, New York, 2001).
[3] N. Kosugi, J. Electron Spectrosc. **144-147**, 1203 (2005).
[4] A. Yagishita, E. Shigemasa, and N. Kosugi, Phys. Rev. Lett. **72**, 3961 (1994).
[5] J. Adachi, N. Kosugi, and A. Yagishita, J. Phys. B **38**, R127 (2005).
[6] Y. Velkov, V. Kimberg, N. Kosugi, P. Sałek, and F. Gel'mukhanov, Chem. Phys. Lett. **476**, 147 (2009).
[7] M. N. Piancastelli *et al*., Phys. Rev. Lett. **88**, 243002 (2002).
[8] I. Hjelte, O. Björneholm, V. Carravetta, C. Angeli, R. Cimiraglia, K. Wiesner, S. Svensson, and M. N. Piancastelli, J. Chem. Phys. **123**, 064314 (2005).
[9] R. Feifel *et al*., J. Chem. Phys. **128**, 064304 (2008).
[10] A. Pietzsch *et al*., Phys. Rev. Lett. **106**, 153004 (2011).
[11] P. Glans, K. Gunnelin, P. Skytt, J. H. Guo, N. Wassdahl, J. Nordgren, H. Ågren, F. K. Gel'mukhanov, T. Warwick, and E. Rotenberg, Phys. Rev. Lett. **76**, 2448 (1996).
[12] M. Oura, O. Takahashi, T. Gejo, T. Tokushimal, Y. Horikawa, Y. Senba, H. Ohashi, and S. Shin, J. Phys. Conf. Ser. **235**, 012016 (2010).
[13] F. Hennies, A. Pietzsch, M. Berglund, A. Föhlisch, T. Schmitt, V. Strocov, H. O. Karlsson, J. Andersson, and J.-E. Rubensson, Phys. Rev. Lett. **104**, 193002 (2010).
[14] T. Tokushima, Y. Harada, O. Takahashi, Y. Senba, H. Ohashi, L.G.M. Pettersson, A. Nilsson, and S. Shin, Chem. Phys. Lett. **460**, 387 (2008).
[15] H. Ohashi *et al*., AIP Conf. Proc. **879**, 523 (2007).
[16] Y. Senba, H. Ohashi, H. Kishimoto, T. Miura, S. Goto, S. Shin, T. Shintake, and T. Ishikawa, AIP Conf. Proc. **879**, 718 (2007).
[17] N. Kosugi, Chem. Phys. **289**, 117 (2003).
[18] N. Kosugi, J. Electron Spectrosc. **137–140**, 335 (2004).
[19] N. Kosugi and H. Kuroda, Chem. Phys. Lett. **74**, 490 (1980).
[20] N. Kosugi, Theor. Chim. Acta **72**, 149 (1987).
[21] P. Sałek, F. Gel'mekhanov, and H. Ågren, Phys. Rev. A **59**, 1147 (1999).
[22] P. Sałek, Comput. Phys. Commun. **150**, 85 (2003).
[23] N. Kosugi, E. Shigemasa, and A. Yagishita, Chem. Phys. Lett. **190**, 481 (1992).
[24] B. R. Lewis, S. T. Gibson, S. S. Banerjee, and H. Lefebvre-Brion, J. Chem. Phys. **113**, 2214 (2000).
[25] S. J. Schaphorst, C. D. Caldwell, M. O. Krause, and J. Jiménez-Mier, Chem. Phys. Lett. **213**, 315 (1993).